position readouts, triggers, and software for processing the data and displaying the results. The updating of this system is now in progress. A significant improvement will come from the change to motors with integral controllers, because the long wires that have been a source of electromagnetic noise in the measurements will be eliminated.

#### *Helmholtz Coil System for Measurement of Individual Magnet Blocks*

The Helmholtz coil system is used for measuring the direction and strength of the total magnetic moment of permanent magnet blocks. Each magnet block that is used in an undulator magnetic structure is measured individually, and the data are used to sort the magnet blocks and determine their arrangement in the assembled device.

The controls and readout of the system have been improved. The old analog integrator was replaced by a fast 16-bit National Instruments ADC on the PCI bus. The integration is now performed digitally. The old electronically noisy stepper motor has been replaced with a servomotor that incorporates electronics for servo-loop feedback. Previously, the magnet block was rotated in 15° steps, but now the measurements are made on-the-fly with a 10 kHz sampling rate. The result is a better signal/noise ratio and more data per turn for precise digital analysis. With the first set of magnets measured after the upgrade, a reproducibility of 3 parts in 10000 was achieved.

## 2.2 Synchrotron Radiation Instrumentation Engineering

The XFD develops instrumentation, beamline components, and front-end components, for SRI CAT, for other CATs, and for the APS facility.

### 2.2.1 Front-End Design for a Canted Undulator Beamline

The XFD has designed a front end for two canted undulator beamlines from a single straight section that will allow greater utilization of the APS (see Fig. 2.11). This design will be used in three new sectors. This front end, vs. 200c, is designed to operate at a maximum beam current of 200 mA with dual 2.07-m-long undulators with a 1 mrad x-ray beam separation at 10.5 mm ID gap (K=2.8). The maximum total power on the front end is 20 kW, and the maximum peak power density is 276 kW/mrad$^2$. Many innovations were made in this front-end design to improve performance and to reduce cost. Figure 2.12 shows a model of the photon shutter (PS1 and PS2). The design was the result of optimizing the cooling and cross section to reduce the mechanical stress from thermal loading. Another redesigned component was the safety shutter. The tungsten block was changed to simplify the geometry to reduce fabrication cost. The wall collimator was also redesigned and the length reduced from 800 mm to 300 mm, which simplifies installation while maintaining adequate shielding thickness. The sizes of most in-line vacuum fittings, such as the tubes and flanges, were reduced—significantly lowering the cost. Most of the pumps are mounted in-line to increase the pumping speed. All of the support tables were redesigned using commercially available extruded aluminum bars to reduce cost.

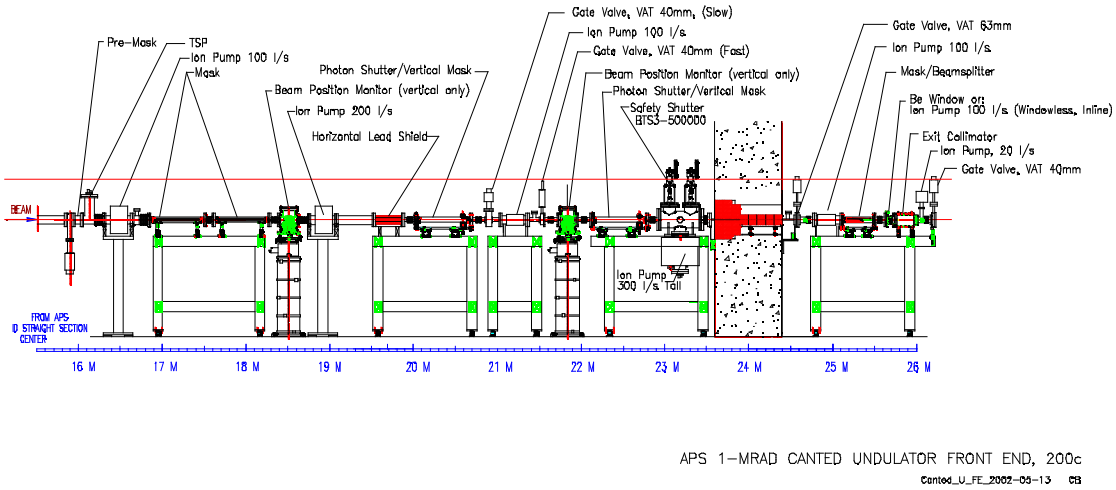


Fig. 2.11. Layout of the new front end for the canted undulator beamlines.

### 2.2.2 Enhanced Heat Transfer Measurements

Methods for enhancing heat transfer in cooling channels have been used and incorporated into all APS front-end (FE) high-heat-load components. In previous FE designs, porous copper mesh inserts with 76% porosity made from 8" × 8" × 0126" copper mesh were brazed into all FE photon-shutter and fixed-mask cooling channels to minimize beam-strike surface temperatures and corresponding thermally induced stresses. Although porous copper mesh inserts offered the best solution at the time, a new heat transfer enhancement technology using wire coils has been developed at the APS. Compared to mesh inserts, wire coils offer high levels of heat transfer enhancement at significantly lower sustained pressure loss. Wire coils are sized to fit snugly inside of the heat transfer testing tube. Due to the tube construction, heat flow is essentially radial, and thus the heat transfer coefficient can be directly calculated using simple one-dimensional heat transfer equations. Figure 2.13 provides heat transfer results for various pitch 0.094" wire coil inserts; data for a standard 76% porosity mesh insert are also included for comparison. All samples were tested in the

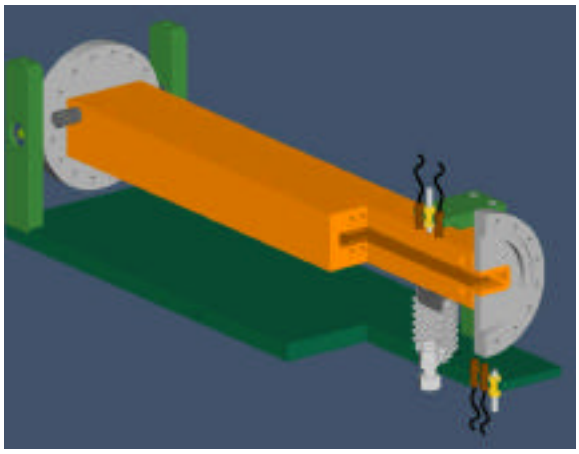

Fig. 2.12. The design of the PS1 and PS2 shutter/mask uses GlidCop beam strike plates brazed to an OFHC body. The bellows actuator eliminates the need for air cylinders with radiation-sensitive seals.

same heat transfer tube, and the results agree, within a few percent across the flow range, with the classic Dittus-Boelter relation ensuring excellent data integrity. Note that the results for the 0.094" wire coil with 0.20" pitch are very close to the standard mesh insert results. However, as can be seen in Fig. 2.14, the corresponding pressure loss results are substantially different from the mesh insert results. At comparable flow rates, the 0.20" wire coil yields nearly four times less pressure loss.

### 2.2.3 ID Vacuum Chamber Development and Fabrication

A family of ID vacuum chambers has been developed over the years at the APS based on extruded aluminum technology.

Chambers with an 8 mm aperture are standard at the APS, but 5 mm and 12 mm aperture chambers have also been designed. The technology has also been extended to provide chambers for BESSY II, in Berlin, Germany, for the Deutsches Elektronen-Synchrotron (DESY) vacuum-ultraviolet free-electron laser, and for the Swiss Light

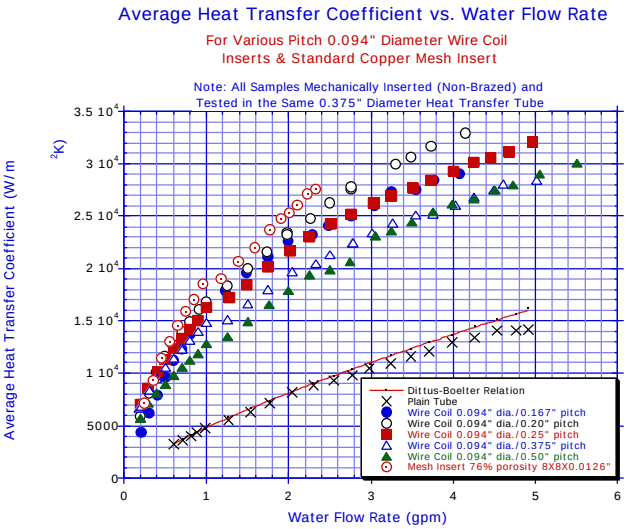


Fig. 2.13. Heat transfer results for various pitch 0.094" wire coil inserts.

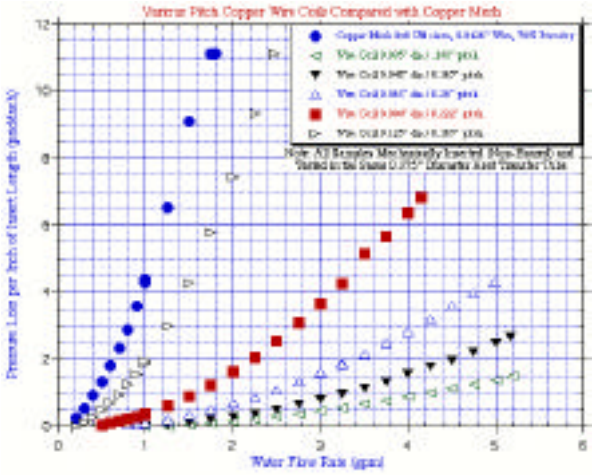


Fig. 2.14. Pressure loss results for various wire coil inserts.

Source at the Paul Scherer Institute. Over the last two years, a new chamber has been designed at the APS with a 7.5 mm aperture and a revised profile that provides greater vertical clearance at the horizontal extremes of the aperture (Fig. 2.15). The new chamber should help to reduce beam loss during injection. A new extrusion has been produced for this cross section, and four new vacuum chambers are being fabricated. The end transition that is welded to the chamber was also be redesigned to allow a more gradual transition from the standard 42 mm ellipse storage ring chamber and thus reduce rf wakefield effects. The new profile chamber will be used for the insertion device vacuum chamber of the new canted undulator beamlines. The straight sections for these beamlines require chambers that include beam position monitors at the center of the chamber between the two undulators in order to decouple beam motion on the second undulator beamline from induced gap changes due to the electron beam motion of the first undulator.

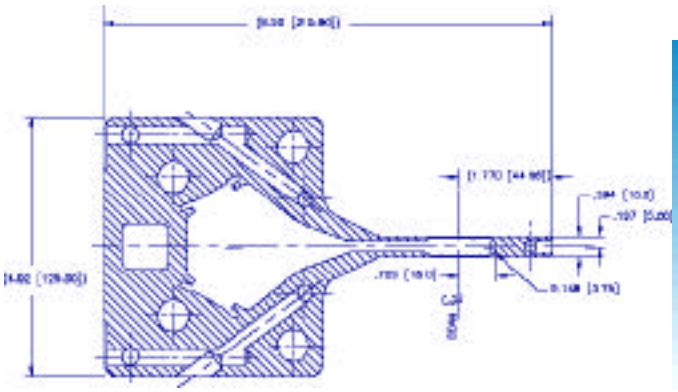

Fig. 2.15. Cross section of the 7.5-mm-aperture ID vacuum chamber. Note the oval beam aperture.

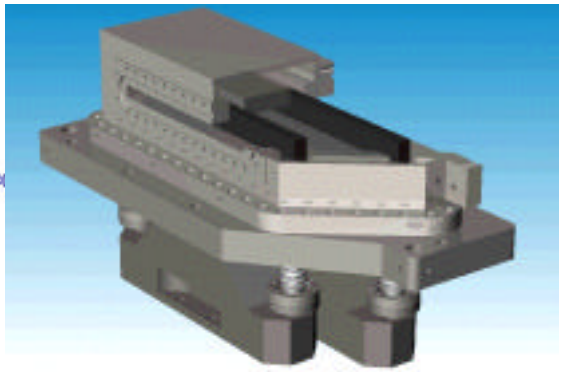

Fig. 2.16. Mono Shutter P8-70.

### 2.2.4 Engineering Support to CATs by XFD

In addition to internal support for SRI CAT, XFD provides design engineering support to other CATs around the storage ring. Typically, this support is for the mechanical design of new standard components or the thermal and stress analysis of existing components.

A major new design was a new mono shutter for the IMM CAT beamline including design changes on the existing hutch to accommodate the shutter. The shutter was designed as a compact unit (Fig. 2.16) capable of providing users with the means of shutting off the beam in multiple secondary beamlines that are at different angles to the primary beamline.

### 2.2.5 Undulator Mechanical Design

One of the consequences of the reduction in the number of poles that characterizes the canted undulator design is a change in the way that ID strongbacks deform under the influence of the attractive force. This in turn influences the magnetic field. In order to better understand the impact of the reduced number of poles on the strongback, an extensive static deformation analysis of the strong-back was performed (Fig. 2.17).

The results of the calculations (Fig. 2.18) indicate that removal of 10 poles on each side of the strongbacks affects gap height in two ways. First, the maximum reduction in gap height reaches twice the value of the gap reduction calculated for the original 144 pole structure but is limited to the central portion of the strongbacks. Second, the ends of the 124 pole strongbacks deflect in the opposite direction than do the ends of the 144 pole strongbacks, and gap height increases towards the ends of the strong-backs. Although the shape of elastic line is changed and the extent of deformation doubles for both 124 pole upper and lower strongbacks, the changes in gap height do not exceed 0.15% of its nominal value. We believe that careful magnetic tuning can eliminate the influence of the strongback deformation on the magnetic field.

### 2.2.6 LCLS Assembly

The XFD is building the prototype undulator for the LCLS project (Fig. 2.19). The LCLS is a proposed fourth-generation light source that will be located at the Stanford Linear

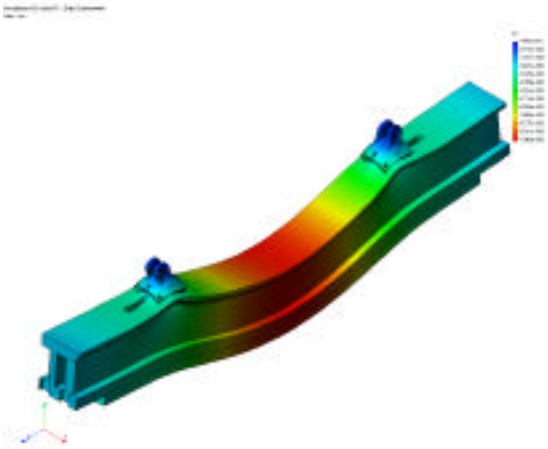

a) 124 pole structure, no stiffeners

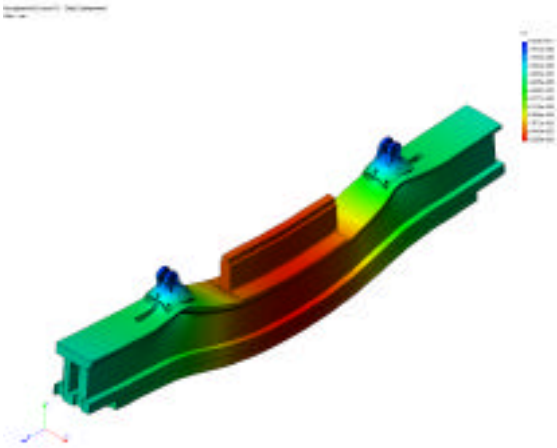

b) 124 pole structure with stiffeners

Fig. 2.17. Y-direction deformation of the upper strongback.

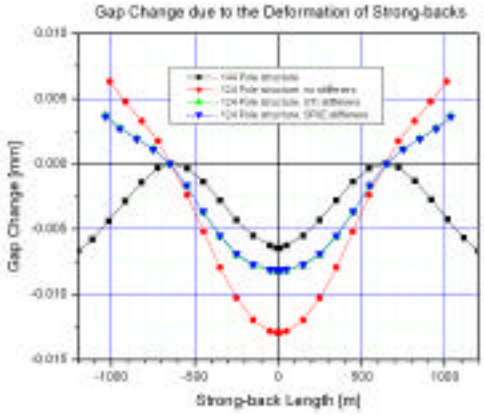


Fig. 2.18. Gap change due to the deformation of strongbacks.

Accelerator Center (SLAC). The 3.4-meter-long permanent magnet undulator is a fixed-gap device with a gap tolerance of +/- 6 microns. To meet this requirement, the strongback is fabricated out of a solid piece of titanium. In addition to its strength, titanium has a low coefficient of thermal expansion. To complete the 3.0-cm-period device, 452 vanadium permendur poles are needed. Upon completion, the poles undergo a thermal stress relief and are individually measured and sorted to adhere to the +/- 3 micron nearest-neighbor pole-gap specification. Likewise, the 450 neodimium iron boron magnets are individually measured to determine the magnetic properties and then sorted. The device is adjusted in both the horizontal and vertical planes using a novel cam-type design whereby servomotors rotate the cylindrical strongback in a specific sequence to achieve the desired location.

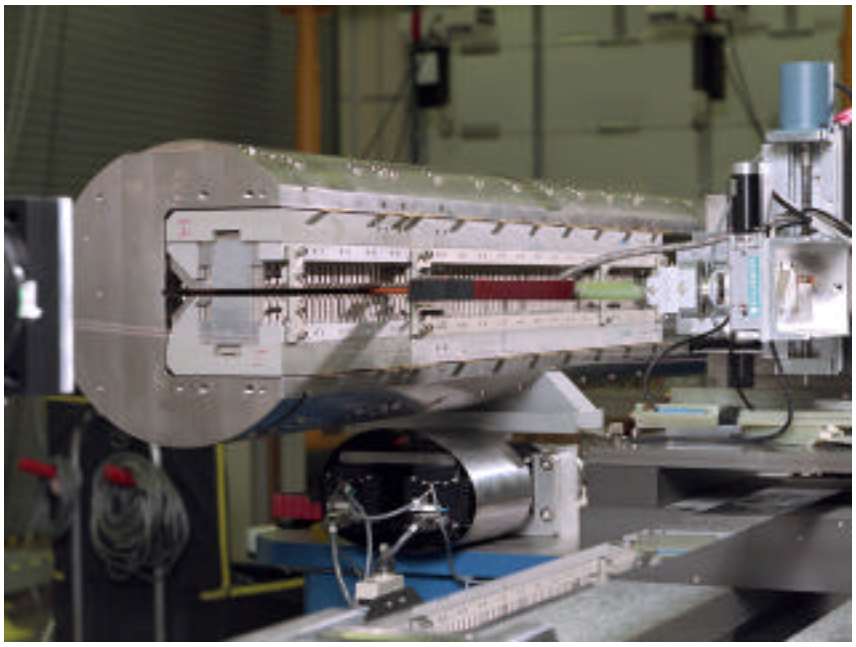

Fig. 2.19. The LCLS prototype undulator on the magnetic measurement bench.

### 2.2.7 4-ID-A BCTF Photon Shutter Simulation Experiments

Most of the original version 1.2 photon shutters have been in operation for over five years. However, it is very difficult if not impossible to obtain sufficient operational data to verify thermal performance due to the extreme radiation present within a front end. Surface temperature mapping in conjunction with thermocouple data is required for proper comparison with a model, but infrared imaging is not possible without destroying the camera in the process due to the radiation. Operational data are needed to determine the maximum thermal load and power density that can be tolerated, and this information is also needed to assess the expected life cycle.

To obtain operational data, a series of experiments is planned in order to simulate a range of thermal loading conditions that might exist on version 1.2 photon shutters. The experiments will be performed in the 4-ID-A beamline components testing facility (BCTF) testing chamber using two primary test pieces. Each test piece will be identical in cross section to the beam strike surface of the version 1.2 photon shutter—but will be much shorter in length. One test piece will contain standard brazed copper mesh inserts, and the other will have open channels. This will bracket the range of heat transfer coefficient values that might exist in operation. The test pieces will be individually mounted, one at a time, inside the BCTF chamber on X-Y-Z stages and a rotational stage in order to precisely control the position and angle of the beam strike surface relative to the beam. Each test piece will be instrumented with a series of thermocouples positioned under the beam strike surface. A large sapphire window will be mounted on the BCTF chamber that will allow direct viewing of the beam strike surface using an infrared camera.

Simultaneous thermocouple data and infrared data will be collected over a range of beam conditions for each of the two test pieces. Coolant water flow rate and enthalpy data for each of the individual coolant channels within the test pieces will also be collected. Valves will be incorporated on each coolant channel's return lines so that the coolant flow rate can be individually set for each channel.

Figure 2.20 shows a cut-away view of the BCTF chamber with the test piece installed. Note that the centerline of the shaft coupling the test piece to the stages corresponds to the beam strike surface, thus the test piece can be rotated with respect to the beam and the beam position will not move with respect to the surface location. Data can be collected for a series of different rotational angles, yielding different power loading conditions, without requiring repositioning of the test piece. This allows for rapid, repeatable data collection over a range of conditions.

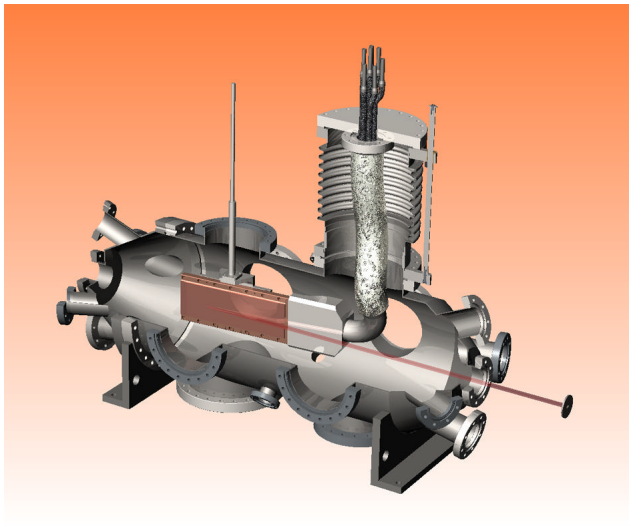

Fig. 2.20. Cut-away view of the test piece for the photon shutter simulation experiments.

In addition to these experiments, spare version 1.2 P1 and P2 blades have been fabricated for the purpose of exchanging these blades with operational shutter blades that have experienced severe duty. Metallurgical examinations will be performed on the blades in order to assess damage in the beam strike zones. This will be the first time that photon shutter blades have been available for metallurgical examination. Photography, stereo microscopy with high-resolution digital imaging, and high-resolution metallography can determine if there is a problem that warrants destructive testing. Examining these shutter blades will develop a procedure for testing present and future front-end high-heat-load components.

### 2.2.8 Software Development

Significant advances have been made in the integration of all steps of a tomography experiment into a single user interface. An easy-to-use, robust user interface has been developed to allow users to “pre-program” the steps necessary to acquire a complete set of tomographic data. Once set up, the data-acquisition process can continue to completion without further user interaction. This step alone has significantly decreased the time required to acquire a complete set of data.

In addition, initial steps have been taken to integrate the preprocessing and reconstruction steps into the same interface. The ultimate goal is to provide the user a single interface through which they can control the many machines and processes required to complete a tomographic experiment.

A stand-alone Linux cluster for parallel processing has also been successfully implemented. A small subset of users routinely use this parallel processing cluster

to perform time-consuming calculations in a fraction of the time required on a single machine. In most cases, users can now take home their processed data within hours of the completion of their experiment rather than take it home and struggle for days to process it themselves. In the future, user interface improvements to this system will open up this capability to all users with a need for processing power.

Improvements and new features have also been added to the CCD acquisition program used by the majority of SRI-CAT users for acquiring CCD data. It is now possible for users to control cameras from five different manufacturers through the same user interface—all seamlessly integrated into the standard EPICS control system. Additional data acquisition modes have been added to make the system more useable to a greater number of people.

## 2.3 X-ray Optic Fabrication and Metrology

The CAT members at the APS continued to make requests for x-ray optics from the staff of the Optics Fabrication and Metrology (OFM) Group. As detailed below, these requests have come in four areas: metrology, thin film deposition, crystal fabrication, x-ray characterization, and mirror design and consulting. Recent highlights include:

- Differential deposition of gold for K-B mirrors was perfected to achieve 0.90 microrad rms deviation over 60 mm from an ideal elliptical surface starting from a spherically shaped silicon substrate.
- Fabrication of a Si crystal designed for sagittal focusing in a bender with a thickness of 0.9 mm over a diffraction area of 53 mm by 76 mm and with a thickness variation of only 5 microns over the entire diffraction area was achieved.
- Parabolic refractory lenses made by extrusion and having a 0.2 mm wall thickness were fabricated very inexpensively and tested at 81 keV to show effective focusing. Such lenses were assembled into a variable focus unit. Subsequently lenses were obtained for which the wall thickness was reduced to 0.1 mm.
- Polishing of silicon to a roughness of 0.09 nm (rms) was accomplished in-house with chemical mechanical polishing.
- Stitching interferometry, which promises to provide precise figure error data for large mirrors over an area, was demonstrated
- A double-multilayer monochromator was made and put into service on beamline 2-BM (Chu et al., 2002).
- Etching of diamond monochromators to remove strain was found to be efficacious (Maj et al., 2002).

### 2.3.1 X-ray Optics Metrology Laboratory

#### *Measurement Requests*

During the last fiscal year, we handled a total of 110 metrology measurement requests out of which 56 originated from the CATs. These included beamline mirrors, multilayers optics, and mirror bender systems. Metrology requests were filled for the following CATs: BESSRC, Bio, CMC, DND, GSECARS, MHATT, SER, SBC, SGX, SRI, and UNI. Requests from non-APS users originated from SNS/IPNS, Fermi Laboratory, and others. In addition, the laboratory continues to provide measurement data to the OFM Group's polishing facility, thus indirectly supporting the users activities. Such measurements are